IEEE Access
Multidisciplinary ⋮ Rapid Review ⋮ Open Access Journal

Received 30 March 2023, accepted 12 April 2023, date of publication 19 April 2023, date of current version 24 April 2023.

Digital Object Identifier 10.1109/ACCESS.2023.3268533

RESEARCH ARTICLE

Power Amplifier Design for 25.1 km Long-Distance Transmission Under 214 km/h High-Speed Movement of Air-to-Ground Wireless Self-Assembled Network Nodes

ZHIFANG WANG[1], QUANZHEN HUANG[2], AND JIANGUO YU[2]
[1]School of Electrical and Information Engineering, Henan University of Engineering, Zhengzhou 451191, China
[2]School of Electronic Engineering, Beijing University of Posts and Telecommunications, Beijing 100876, China

Corresponding author: Zhifang Wang (wangzf124@haue.edu.cn)

This work was supported in part by the Doctoral Incubation Fund of Henan University of Engineering under Grant D2022011; in part by the National Natural Science Foundations of China under Grant 62173126, Grant 61821001, and Grant 62127802; in part by the Central Plains Science and Technology Innovation Leader Support Program under Grant 234200510027; in part by the Henan University Science and Technology Innovation Team Support Program under Grant 21IRTSTHN017; and in part by the Research Incubation Fund Project of Henan College of Engineering under Grant PYXM202102.

ABSTRACT In this paper, we design a power amplifier for this network protocol to combat the Doppler effect caused by the high-speed movement of network nodes and the rapid signal fading failure caused by the long-distance transmission of network nodes, and to extend the communication distance between network nodes, to realize the long-distance transmission under the high-speed movement of network nodes. The overall design of the power amplifier for bi-directional transmission structure, power amplifier transmitter, and low-noise amplifier receiver is used in a four-stage cascade current series negative feedback structure mode, where the signal transmitter selected RFPA5208 and MAX4003 chip, the signal receiver selected TQP3M9037 and SKY16602 chip. The above overall design enables the self-assembled nodes to ensure stable topology and achieve long-spacing transmission even in the high-speed mobile state. The test results show that the output power is 41.5dBm-44.3dBm, the gain is 44dB-45dB, and the noise is 1.6dB when the frequency band range is 2.4GHz-2.5GHz. The experimental results show that when the self-assembling nodes maintain the relative speed of 214km/h, the longest transmission distance of the point-to-point of the amorphous flat terrestrial wireless self-assembling network reaches 16300m, and the longest transmission distance of the point-to-point of the amorphous flat air-to-ground wireless self-assembling network reaches 25100m. The power amplifier designed in this paper has good application value. It provides an individual research basis for future research on the framework of a low-altitude economic fly-by-wire network.

INDEX TERMS Amorphous flat, air-to-ground wireless ad-hoc network system, 4G/5G bidirectional power amplifier, long-distance transmission of nodes, self-organizing network nodes move at high speed.

I. INTRODUCTION

With the phasing out of 3G [1] equipment, 4G [2] equipment continues to be updated, 5G [3], [4] systems are widely deployed, and 6G [5], [6] technology continues to break through. Users have higher demands on today's wireless communication systems [7], [8], [9]. Achieving long-spacing wireless signal transmission while maintaining the high-speed movement of self-assembled wireless nodes has become a research hotspot and a complex problem.

The above problem is now decomposed into two issues: (1) High-speed movement of self-assembling wireless nodes [10], [11], [12], [13], [14], [15]. (2) Long-distance transmission of self-organizing wireless nodes [16], [17]. Whether problem (1) or problem (2), the premise is that the wireless nodes should form a self-organizing structure.

The associate editor coordinating the review of this manuscript and approving it for publication was Barbara Masini.

This fundamental work can only be implemented by the routing protocol of a self-organizing network [18], [19]. This paper uses CC2530 [20], [21] self-organizing network chip to realize the self-organizing structure of nodes, which uses 802.15.4 (Zigbee) self-organizing network protocol [22], [23], which enables multiple wireless nodes to form a self-organizing network structure automatically. Immediately after, for problem (1), the high-speed movement of wireless self-networking nodes can currently be achieved by both software and hardware, and the software side can improve the threshold of the wireless networking node movement speed by changing the routing protocol of the wireless self-networking nodes, which in turn can achieve high-speed movement. The hardware side can be achieved by adding a very stable high gain antenna [24], [25], [26] or by adding a power amplifier [28], [29] at the RF output [27] that is suitable for this self-organizing wireless node. For problem (2), it would be a great idea to use the currently existing cellular networks [30], [31] and Wi-Fi self-assembling networks [32], [33], [34] as the basis for the study of the long-spacing transmission of wireless networking nodes. Still, both of them have insurmountable problems and difficulties. For example, although the spectrum efficiency [35], [36], [37] is high and widely used when cellular network signals are transmitted, it is a fixed network centered on towers, which requires long-time planning and construction and consumes a lot of human and material resources. Another example is Wi-Fi self-assembling network. Although simple, convenient, and stable transmission, its propagation distance is short, and it is not widely used in the application of long-spacing transmission of nodes, and the current theoretical research is biased. In summary, the design of matching power amplifiers is a good entry point based on the existing networking nodes or network protocols. Currently, research on power amplifiers focuses on output power [38], [39], linearity [40], [41], efficiency [42], [43], and wide bandwidth [44], [45]. Most of the power amplifiers in the market are single amplified transmissions, with the focus limited to low-noise amplifiers or power amplifiers, i.e., the open-loop effect [46], [47], mainly for 802.11.b/g/n protocols [48]. In addition, the current research on self-assembling wireless networks primarily focuses on terrestrial wireless self-assembling networks. Air-ground self-assembling networks are currently mainly applied in the simulation stage and have not been widely put into practical applications.

The framework of an amorphous flattened air-ground self-organizing network system [49] adopted in this paper (whose overall network protocol is adapted to allow the self-organizing nodes to transmit at a certain distance at a certain speed), a 4G/5G bidirectional power amplifier applicable to this network architecture and protocol is designed, which enables the self-organizing wireless nodes to achieve long spacing transmission despite high-speed movement. It has The power amplifier has good application value. This paper provides some primary conditions for the higher requirements faced by wireless communication transmission. Also, it provides some basis for future research on the framework of low-altitude economic fly-by-network. However, there are still some shortcomings, such as how to integrate the wireless self-assembling network nodes and power amplifiers to form a whole is still a problem that needs to be optimized.

II. OVERALL FRAMEWORK STRUCTURE AND CORE PARAMETERS

A. OVERALL FRAME CONSTRUCTION

First, referring to the literature [50], [51], [52], [53], [54], [67], the model for long-range transmission of signals from amorphous flattened wireless self-assembling nodes in free space can be obtained as shown in the equation (1).

$$P_r = \frac{P_t G_t G_r \lambda^2}{(4\pi d)^2 L} \tag{1}$$

In equation (1), P_r is the power received by the wireless self-networking node. P_t is the power transmitted by the wireless self-networking node when it is the signal source. G_t is the antenna gain at the signal transmitting end of the wireless self-organizing node. G_r is the antenna gain at the signal-receiving end of the self-assembling wireless node. λ is the wavelength. d is the communication distance between network nodes. L is a constant. If the antenna gain at the transceiver is fixed, equation (1) is rewritten as equation (2).

$$P_r = A_1 \cdot \frac{P_t}{d^2} \tag{2}$$

In equation (2), A_1 is a constant. And the overall framework structure of the long-distance transmission of self-assembled nodes is shown in figure 1

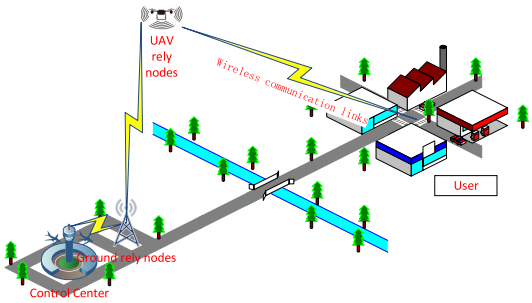

FIGURE 1. Long-range transmission framework of amorphous flattened air-to-ground wireless self-organizing network nodes.

From figure 1, it can be seen intuitively that the control center sends out relevant control commands and transmits the command signals to the users through the relay complementary blind transmission of the joint relay nodes (including the ground relay nodes and the air relay nodes), finally achieving the purpose of long-distance communication. Secondly, as the self-assembled network nodes move at high speed, which will inevitably produce the Doppler effect, then there are references [55], [56], [57], [58], the energy consumption model of the self-assembled network nodes in the process

of moving at high speed can be obtained as shown in equation (3).

$$P_r = A_2 \cdot \frac{P_t}{d^{\alpha}} \tag{3}$$

In equation (3), P_r is the power received by the signal host network node. P_t is the energy emitted by the source network node. d is the communication distance between the network nodes. α is the path loss index. Then, the final power received by the node with the messaging host network is shown in equation (4).

$$P_{rf} = P_t - \beta P_t - P_1 - P_2 \tag{4}$$

In equation (4), P_{rf} is the final power received by the signal host network node. P_t is the energy emitted by the source node. β is the power loss factor. P_1 is the possible power loss of each network node. P_2 is the other possible power loss. The overall framework structure of the self-organizing network node for high-speed mobility is shown in figure 2

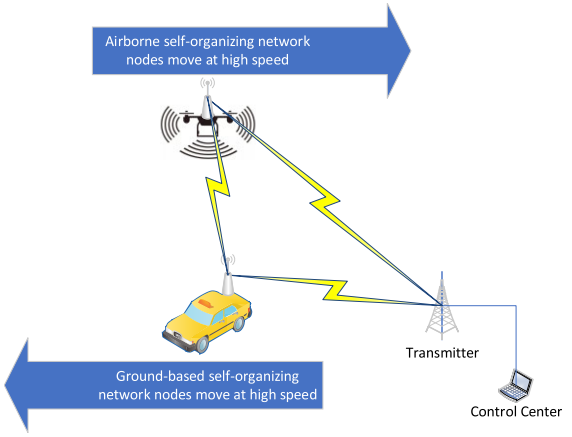

FIGURE 2. High-speed mobile transmission framework of amorphous flattened air-to-ground wireless self-assembly nodes.

Figure 2 shows that the control center sends out relevant control commands and transmits the command signals to the air network nodes and the ground network nodes through the transmission nodes. The comprehensive equation (1-4) can be seen that when the antenna gain of the transceiver end of the amorphous flattened air-to-ground wireless self-assembly network system is fixed, for the long-distance transmission in the high-speed mobile state of the wireless self-assembly network node, the power received by the wireless self-assembly network letter host node is inversely proportional to the square of the communication distance, and is proportional to the transmitting power size of the wireless self-assembly network signal source node, then there is in order to In order to achieve the purpose that the wireless self-organizing network nodes can maintain long-distance transmission even in the high-speed mobile state, it is necessary to increase the power of both the transmitting end of the signal source and the receiving end of the signal host node, so that the high-gain bidirectional power amplifier conforming to the amorphous flat wireless self-organizing network protocol should be connected to each networking node. Therefore, how to design a high-gain bidirectional power amplifier that meets the requirements is the focus of this paper.

B. FOUR-STAGE CASCADED NEGATIVE CURRENT FEEFBACK CIECUIT MODEL

The 4G/5G bi-directional power amplifier designed in this paper has an overall bi-directional transmission structure. The forward transmission is a PA (power amplifier), intended to amplify the transmit power of the source networking node and enhance the signal transmission strength. The reverse transmission is LNA (low noise amplifier), designed to receive and amplify the signals from the joint relay network nodes (including the ground relay network nodes and the air relay network nodes). Both PA and LNA adopt a four-stage cascade structure, and each stage is configured with a current series of negative feedback. This paper uses the PA as an example for theoretical performance analysis, and the LNA can be analogous. Among them, the block diagram of the four-stage cascade structure of PA is shown in figure 3.

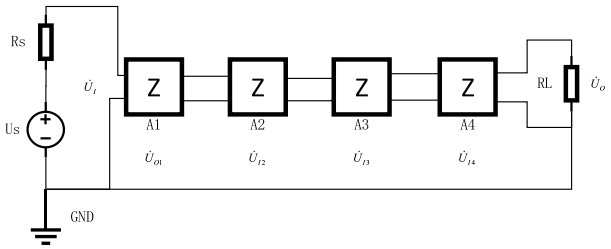

FIGURE 3. Block diagram of the four-stage cascade structure of PA.

From figure 3: The output voltage of the amplifier circuit's pre-stage is the post-stage's input voltage, as shown in equation (5).

$$\begin{cases} U_{O1} = U_{I2} \\ U_{O2} = U_{I3} \\ U_{O3} = U_{I4} \end{cases} \tag{5}$$

Then there is a four-stage amplifier circuit with voltage amplification, as shown in equation (6).

$$\begin{aligned} \dot{A}_U &= \frac{\dot{U}_O}{\dot{U}_I} \cdot \frac{\dot{U}_{O1}}{\dot{U}_I} \cdot \frac{\dot{U}_{O2}}{\dot{U}_{I2}} \cdot \frac{\dot{U}_{O3}}{\dot{U}_{I3}} \cdot \frac{\dot{U}_O}{\dot{U}_{I4}} \\ &= \dot{A}_{U1} \cdot \dot{A}_{U2} \cdot \dot{A}_{U3} \cdot \dot{A}_{U4} \end{aligned} \tag{6}$$

And,

$$\dot{A}_U = \prod_{i=1}^{4} \dot{A}_{Ui} \tag{7}$$

From equation (7), the voltage magnification of the four-stage amplifying circuit is equal to the product of the voltage magnifications of the various stages of the amplifying course that compose it. For the first stage to the fourth stage, the amplification of each step should be when the input resistance of the next stage is used as the load. The four-stage amplifying

circuit's input resistance should be the first stage's input resistance, as shown in equation (8).

$$R_I = R_{I1} \tag{8}$$

The output resistance of the four-stage amplifying circuit should also be the input resistance of the first-stage amplifying circuit, as shown in equation (9).

$$R_O = R_{O1} \tag{9}$$

From the above analysis, it can be obtained that the amplification of the four-stage amplification circuit at all levels are: $\dot{A}_{U1}, \dot{A}_{U2}, \dot{A}_{U3}, \dot{A}_{U4}$, then there are corresponding logarithmic amplitude-frequency characteristics and phase-frequency characteristics as shown in equation (10).

$$\begin{cases} 20\lg\left|\dot{A}_U\right| = \sum_{i=1}^{4} 20\lg\left|\dot{A}_{Ui}\right| \\ \varphi = \sum_{i=1}^{4} \varphi_i \end{cases} \tag{10}$$

Next, without considering the essential design factors, assume that the four-stage power amplifier circuit designed in this paper has the same frequency response, as shown in equation (11).

$$\begin{cases} \dot{A}_{U1} = \dot{A}_{U2} = \dot{A}_{U3} = \dot{A}_{U4} \\ \dot{A}_{UM1} = \dot{A}_{UM2} = \dot{A}_{UM3} = \dot{A}_{UM4} \\ f_{L1} = f_{L2} = f_{L3} = f_{L4} \\ f_{H1} = f_{H2} = f_{H3} = f_{H4} \end{cases} \tag{11}$$

In equation (11), $\dot{A}_U$ indicates the circuit amplification. $\dot{A}_{UM}$ denotes the IF voltage gain. f_L indicates the lower cutoff frequency. f_H indicates the upper cutoff frequency. Then there is the IF voltage gain of the whole four-stage circuit, as shown in equation (12).

$$\begin{aligned} 20\lg\left|\dot{A}_U\right| &= 20\lg\left|\dot{A}_{UM1}\cdot\dot{A}_{UM2}\cdot\dot{A}_{UM3}\cdot\dot{A}_{UM4}\right| \\ &= 80\lg\left|A_{UM1}\right| \end{aligned} \tag{12}$$

When $f = f_{L1}$, we can get equation (13).

$$\begin{cases} \dot{A}_{U1} = \dot{A}_{UL1}, \dot{A}_{U2} = \dot{A}_{UL2} \\ A_{U3} = \dot{A}_{UL3}, A_{U4} = \dot{A}_{UL4} \end{cases} \tag{13}$$

And,

$$\begin{cases} \left|\dot{A}_{UL1}\right| = \left|\dot{A}_{UL2}\right| = \frac{\left|\dot{A}_{UM1}\right|}{\sqrt{2}} \\ \left|\dot{A}_{UL3}\right| = \left|\dot{A}_{UL4}\right| = \frac{\left|\dot{A}_{UM3}\right|}{\sqrt{2}} \end{cases} \tag{14}$$

And,

$$20\lg\left|\dot{A}_U\right| = 80\lg\left|A_{UM1}\right| - 80\lg\sqrt{2} \tag{15}$$

In equation (15), When the amplifier gain drops by 6 dB, and since both $\dot{A}_{U1}, \dot{A}_{U2}$ and $\dot{A}_{U3}, \dot{A}_{U4}$ produce an additional phase shift of $+45°$, then $\dot{A}_U$ produces a different phase shift of $+180°$. Similarly, when $f = f_{H1}$, the other phase shift is $-180°$ for the same 6 dB drop in gain. This is followed by an analysis of the designed four-stage power amplifier's upper cutoff frequency and lower cutoff frequency. First, for the lower cutoff frequency, substitute $\dot{A}_{Ui}$ in equation (7) with the expression for the low-frequency amplification $\dot{A}_{ULi}$ and take the mode, as shown in equation (16).

$$\left|\dot{A}_{UL}\right| = \prod_{i=1}^{4} \frac{\left|\dot{A}_{UMi}\right|}{\sqrt{1+\left(\frac{f_{Li}}{f}\right)^2}} \tag{16}$$

When $f = f_{L1}$, we can get equation (17).

$$\left|\dot{A}_{UL}\right| = \prod_{i=1}^{4} \frac{\left|\dot{A}_{UMi}\right|}{\sqrt{2}} \tag{17}$$

And,

$$\prod_{i=1}^{4} \sqrt{1+\left(\frac{f_{Li}}{f}\right)^2} = \sqrt{2} \tag{18}$$

The simultaneous squaring of both sides of the equation (18) leads to equation (19).

$$\begin{aligned} &\left(1+\left(\frac{f_{L1}}{f}\right)^2\right)\left(1+\left(\frac{f_{L2}}{f}\right)^2\right) \\ &\times\left(1+\left(\frac{f_{L3}}{f}\right)^2\right)\left(1+\left(\frac{f_{L3}}{f}\right)^2\right) = 2 \end{aligned} \tag{19}$$

And,

$$1 + \sum\left[1+\left(\frac{f_{L1}}{f}\right)^2\right] + o\left[1+\left(\frac{f_{L1}}{f}\right)^4\right] = 2 \tag{20}$$

In equation (20), $o\left[1+\left(\frac{f_{L1}}{f}\right)^4\right]$ is a higher-order infinitesimal of $\sum\left[1+\left(\frac{f_{L1}}{f}\right)^2\right]$, so since $\frac{f_{Li}}{f} < 1$, then, we have $o\left[1+\left(\frac{f_{L1}}{f}\right)^4\right] \to 0$, which can be neglected. Then we can get equation (21).

$$f_L \approx \sqrt{\sum f_{Li}^2} \tag{21}$$

Referring to the literature [59] and correcting the relevant parameters, we can obtain equation (22).

$$f_L \approx \frac{11}{10}\sqrt{\sum f_{Li}^2} \tag{22}$$

Next, for the upper cut-off frequency, the same can be obtained by substituting an in equation (7) with the expression for the low-frequency amplification b and taking the modulus, as shown in equation (23).

$$\left|\dot{A}_{UH}\right| = \prod_{i=1}^{4} \frac{\left|\dot{A}_{UMi}\right|}{\sqrt{1+\left(\frac{f_{Hi}}{f}\right)^2}} \tag{23}$$

When $f = f_H$, then we can get equation (24).

$$|\dot{A}_{UH}| = \prod_{i=1}^{4} \frac{|\dot{A}_{UMi}|}{\sqrt{2}} \tag{24}$$

And,

$$\prod_{i=1}^{4} \sqrt{1 + \left(\frac{f_H}{f_{Hi}}\right)^2} = \sqrt{2} \tag{25}$$

The simultaneous squaring of both sides of equation (25) yields equation (26).

$$\left(1 + \left(\frac{f_H}{f_{H1}}\right)^2\right)\left(1 + \left(\frac{f_H}{f_{H2}}\right)^2\right) \times \left(1 + \left(\frac{f_H}{f_{H3}}\right)^2\right)\left(1 + \left(\frac{f_H}{f_{H4}}\right)^2\right) = 2 \tag{26}$$

The approximate expression of equation (26) is equation (27).

$$\left(\frac{1}{f_H}\right)^2 = \sum_{i=1}^{4} \left(\frac{1}{f_{Hi}}\right)^2 \tag{27}$$

Referring to the literature [59] and correcting the relevant parameters, we can obtain equation (28).

$$\frac{1}{f_H} \approx \frac{11}{10} \sqrt{\sum \left(\frac{1}{f_{Hi}}\right)^2} \tag{28}$$

Then the upper and lower limit frequencies of the four-stage amplifier circuit with the same frequency are shown in equation (29).

$$\begin{cases} f_H \approx 0.455 f_{H1} \\ f_L \approx 2.2 f_{L1} \end{cases} \tag{29}$$

The above are theoretical calculations, and the specific passband also needs to select the relevant chip module for comprehensive analysis. In addition, To suppress the zero-point drift (Q-point drift) phenomenon generated by the capacitor inductor in the high-frequency circuit in this 4G/5G bidirectional power amplifier, a current series negative feedback circuit is further added to each stage of the amplifier circuit in figure 3, and the designed circuit block diagram is shown in figure 4.

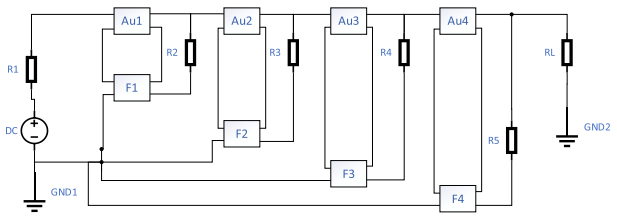

FIGURE 4. PA circuit block diagram.

In figure 4, $A_{u1}, \ldots, A_{u4}$ denote the amplifier circuit of the 4G/5G bi-directional power amplifier, respectively. $F_1, \ldots, F_4$ represent the current negative feedback circuit corresponding to the 4G/5G bi-directional power amplifier's amplifier, respectively. Next, the PA circuit block diagram in figure 4 is analyzed. And first defined as follows, let $\dot{Q}_i$ be the circuit input, $\dot{X}_f$ be the circuit feedback, and $\dot{Q}_{i0}$ be the net circuit input. Then, as shown in equation (30).

$$\dot{Q}_{i0} = \dot{Q}_i - \dot{X}_{f1} - \dot{X}_{f2} - \dot{X}_{f3} - \dot{X}_{f4} \tag{30}$$

The amplification of the primary amplifier circuit in figure 4 is shown in equation (31).

$$\dot{A} = \frac{\dot{Q}_{o1}}{\dot{Q}_{i0}} \cdot \frac{\dot{Q}_{o2}}{\dot{Q}_{i0}} \cdot \frac{\dot{Q}_{o3}}{\dot{Q}_{i0}} \cdot \frac{\dot{Q}_{o4}}{\dot{Q}_{i0}} \tag{31}$$

The feedback coefficient is shown in equation (32).

$$\dot{F} = \frac{\dot{X}_{f1}}{\dot{Q}_{o1}} \cdot \frac{\dot{X}_{f2}}{\dot{Q}_{o2}} \cdot \frac{\dot{X}_{f3}}{\dot{Q}_{o3}} \cdot \frac{\dot{X}_{f4}}{\dot{Q}_{o4}} \tag{32}$$

The amplification of the negative feedback amplifier circuit is shown in equation (33).

$$\dot{A}_F = \frac{\dot{Q}_{o1}}{\dot{Q}_i} \cdot \frac{\dot{Q}_{o2}}{\dot{Q}_i} \cdot \frac{\dot{Q}_{o3}}{\dot{Q}_i} \cdot \frac{\dot{Q}_{o4}}{\dot{Q}_i} \tag{33}$$

The loop amplification of the above circuit is shown in equation (34).

$$\dot{A}_F \cdot \dot{F} = \frac{\dot{X}_{f1} \cdot \dot{X}_{f2} \cdot \dot{X}_{f3} \cdot \dot{X}_{f4}}{\left(\dot{Q}_i\right)^4} \tag{34}$$

In summary, equation (35) is further obtained.

$$\dot{A}_F = \frac{\dot{Q}_{o1} \cdot \dot{Q}_{o2} \cdot \dot{Q}_{o3} \cdot \dot{Q}_{o4}}{\left(\dot{Q}_{i0} + \dot{X}_{f1} \cdot \dot{X}_{f2} \cdot \dot{X}_{f3} \cdot \dot{X}_{f4}\right)^4} == \frac{\dot{A}}{1 + \dot{A}\dot{F}} \tag{35}$$

For further simplification results, please refer to the literature [67], which this paper will not describe in detail. Through the analysis of the simplified results in the literature [67], when a four-stage cascade amplifier circuit introduces a four-stage current series deep negative feedback, the magnitude of the circuit amplification almost depends on the design of the matching feedback network circuit, independent of the primary amplifier circuit, i.e., the selected chip module is essential, but how to design the matching circuit with it is more important. The next step is to create the corresponding primary matching circuit for the selected chip module. The basic matching circuit block diagram of one of the core components, PA and LNA, is shown in figure 5. Taking PA as an example, the primary circuit schematic is shown in figure 6. The overall core circuit schematic of PA and LNA is shown in figure 7.

From figure 5, the control center sends out the wireless self-assembling node control command signal as the initial signal source, and the initial signal source is input to the power amplifier through the RF input interface, and then input to the PA through the RF single knife double-throw switch control to realize the signal amplification of the signal source. The filter filters the amplified signal to filter other irrelevant interference noise. Finally, it is controlled by RF single-die double-throw switch again, and the antenna

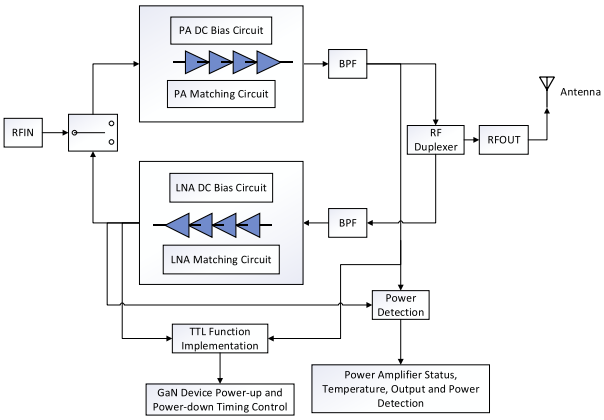

FIGURE 5. Block diagram of the primary matching circuit of PA and LNA.

sends the signal to the target signal host node. At the same time, the signal received from the antenna to the host node is controlled by the RF single-drop switch and input to the Berkeley packet filter for noise filtering. The filtered signal is fed to the LNA, which amplifies the weak signal. The amplified signal is again controlled by the RF single knife double-throw switch and sent to the wireless self-configuration node via the RF input interface, which is finally fed back to the computer control center. Thus, through the above structure power amplifier achieves the signal source node to the signal host node signal complete two-way loop transmission process. The above-structured power amplifier thus achieves comprehensive bi-directional feedback of the signal from the host node. The power detection and timing control modules are connected to the outputs of the PA and the LNA. Among them, the power detection module is used to detect the signal filtered by the filter to get the power amplifier's status, temperature, and output power. The timing control module implements the TTL function and performs timing control.

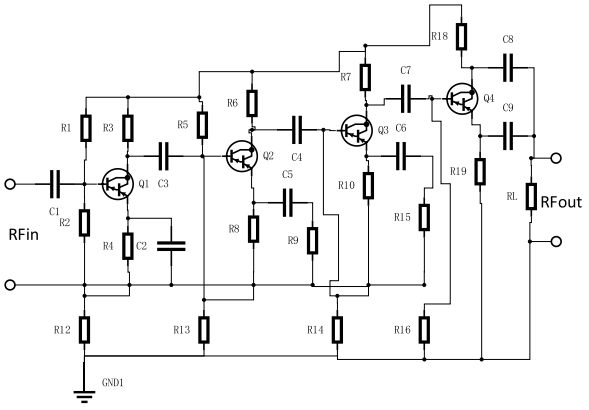

FIGURE 6. Basic circuit schematic.

As can be seen from figure 6 and figure 7: The RFPA5208 chip is used as the core of the PA to amplify the signal source signal. After the source signal enters the PA through the RF input interface, it is amplified by the RFPA5208 chip

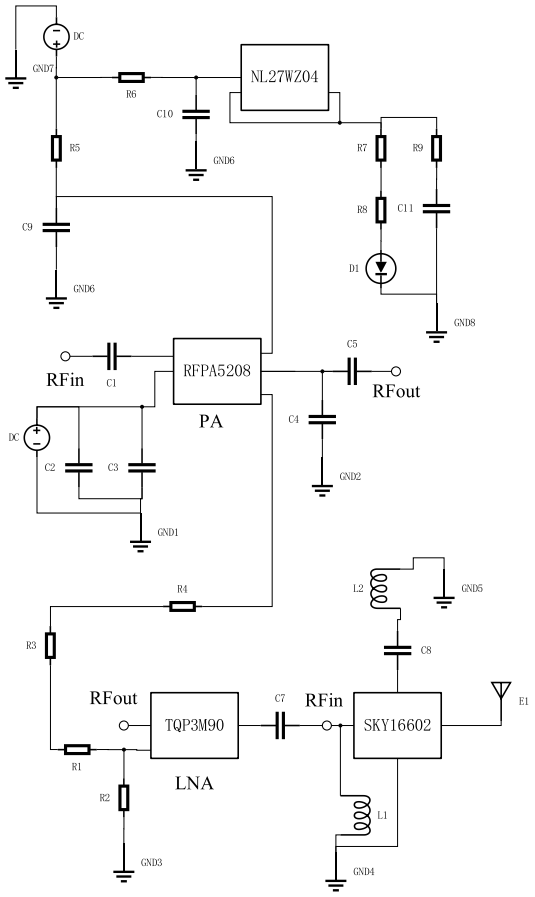

FIGURE 7. The overall core circuit schematic of PA and LNA.

and finally output from the RF output interface. Capacitors C1 and C5 isolate the DC circuit at the RF input and work of the chip RFPA5208, respectively. Capacitor C4 provides RF ground for filtering spurious low-frequency signals. The TQP3M90 and SKY16602 chips are combined in the LNA to process the received network signals. The TQP3M90 chip is used to amplify the received signals from other nodes that are not sensitive to the network. The antenna transmits the received signals from other networking nodes through chip SKY16602 to the RFIN side of the TQP3M90 chip, which is then amplified and processed by chip TQP3M90 and output from the RFOUT port. The capacitor C8 and RF choke L2 are connected in series as RF ground to filter the spurious signals together. L2 is used to suppress the transmission noise of VHF signals or the interference of radiation noise. RF choke L1 RF ground for suppressing transmission noise or radiation noise interference of VHF signals. Capacitor C7 is used to isolate the DC circuit at the RF output of chip TQP3M90. Resistors R1 and R2 are connected in parallel to form a hostile feedback circuit network, which provides a stable output current. Resistors R1, R3, and R4 are connected in series to provide the required voltage feedback signal. NL27WZ04 chip, as a high-performance dual inverter, can significantly reduce the current load on the input driver, and its TTL-compatible output can improve the switching noise function. The signal

amplified by chip RFPA5208 passes through a first-stage circuit, followed by a second-stage circuit, processed by chip NL27WZ04 dual inverter, and RF grounded by a third-stage circuit. The first stage is a parallel circuit with resistor R5 and capacitor C9. R5 forms a negative feedback circuit network to provide stable output current, and C9 provides RF grounding and filters out spurious signals. The second stage circuit is a parallel circuit with resistor R6 and capacitor C10: R6 forms a negative feedback circuit network to provide stable output current, and C10 also provides RF grounding to filter low-frequency signal noise interference. The third stage circuit is a series circuit with resistor R7, resistor R8, voltage regulator diode D1, and a parallel circuit with R9 and capacitor C11. R7, R8, and R9 form a negative feedback circuit network to provide a stable output current, C11 provides RF ground to filter out spurious signals, and D1 ensures that the voltage remains constant. In contrast, the current varies over a wide range.

Then there is the power amplifier top design PCB layout, as shown in figure 8.

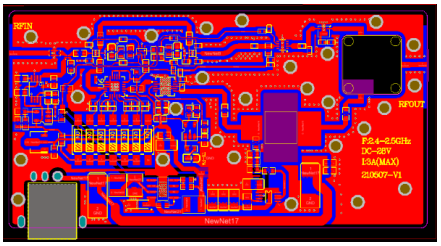

FIGURE 8. Top PCB layout.

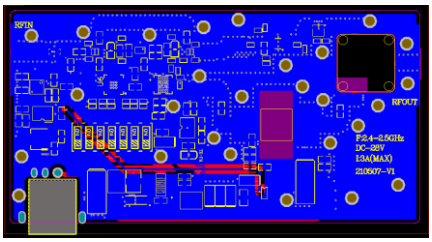

FIGURE 9. Bottom PCB layout.

The PCB layout of the power amplifier bottom layer design is shown in figure 9.

In addition, the physical diagram of the power amplifier designed in this paper for an amorphous flat-space wireless self-assembly network is shown in figure 10.

FIGURE 10. Power amplifier physical drawing.

III. SIMULATION ANALYSIS

This simulation uses ADS2020 software for simulation. The simulation band is set to 1-3GHz, the center frequency is 2.45GHz, and the simulation step is set to 10MHz. Then there are related simulation diagrams as shown in figure 11-figure 18. One of the LNA-related simulation diagrams is shown in figure 11-figure 14.

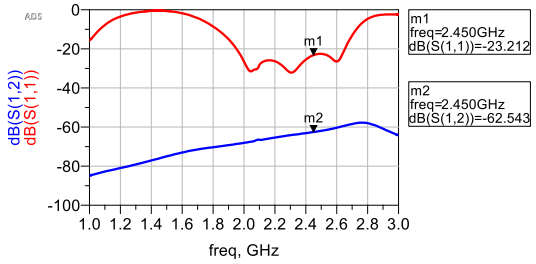

FIGURE 11. Return loss at input and output of LNA.

As shown in figure 11, when the center frequency is 2.45 GHz, the return loss at the input and output of the LNA is −23.212 dB and -62.543 dB, respectively.

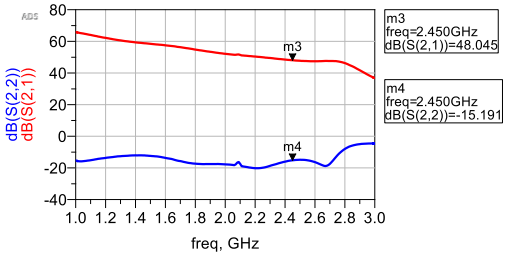

FIGURE 12. Insertion loss at the input and output of LNA.

As shown in figure 12, the insertion loss at the information and work of the LNA is 48.045 dB and −15.191 dB, respectively, when the center frequency is 2.45 GHz.

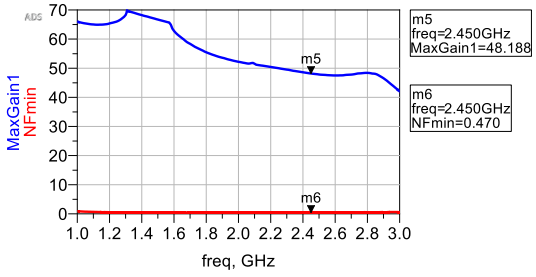

FIGURE 13. Noise gain and maximum gain of LNA.

As shown in figure 13, when the center frequency is 2.45GHz, the maximum gain is 48.188dB, and the noise is 0.47dB. To make the designed power amplifier with generality, when testing its stability, the test frequency is set to 1GHz-3GHz, as shown in figure 14.

As shown in figure 14, when the center frequency is 2.45 GHz, the stability factor is 2.665 $>$ 1, ensuring that the power amplifier's low-noise amplified receiver is stable in the operating band range. The other PA-related simulation diagrams are shown in figure 15-figure 18.

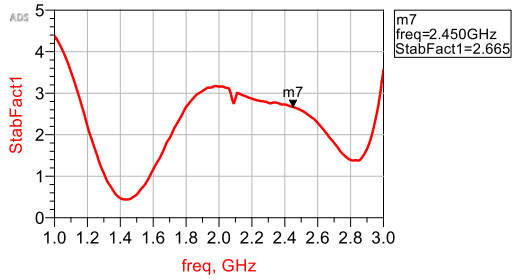

FIGURE 14. Stability coefficient of LNA.

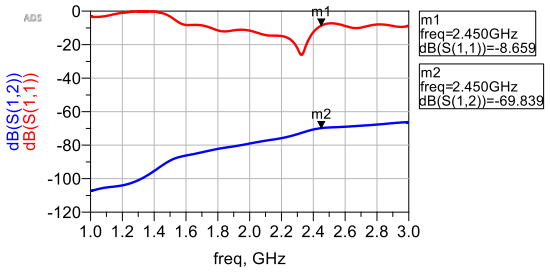

FIGURE 15. Return loss at the input and output of PA.

As shown in figure 15, when the center frequency is 2.45 GHz, the return loss at PA input and output is −8.659 dB and −69.839 dB, respectively.

As shown in figure 16, when the center frequency is 2.45 GHz, the insertion loss at the PA input and output is 55.115 dB and −7.296 dB, respectively.

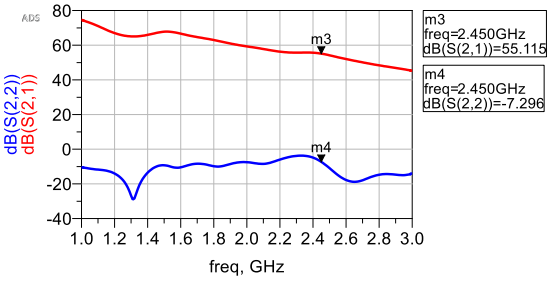

FIGURE 16. Insertion loss at the input and output of PA.

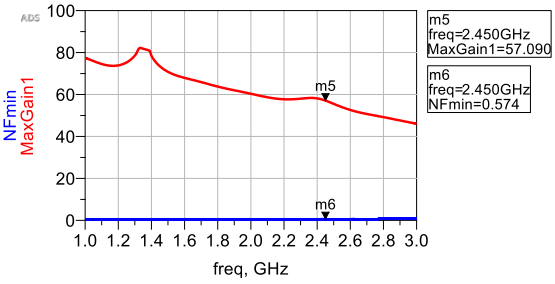

FIGURE 17. Noise gain and maximum gain of PA.

As shown in figure 17, when the center frequency is 2.45GHz, the maximum gain is 57.090dB, and the noise is 0.574dB. To make the designed power amplifier with generality, when testing its stability, the test frequency is set to 1GHz-3GHz, as shown in figure 18.

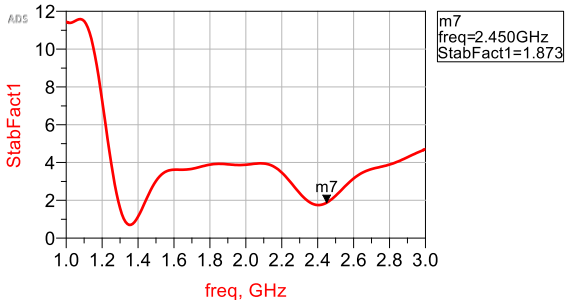

FIGURE 18. Stability coefficient of LNA.

As shown in figure 18, when the center frequency is 2.45 GHz, the stability coefficient is 1.873>1, which ensures that the power amplifier's power amplification band is stable in the operating band range. The actual test diagram is shown in figure 19.

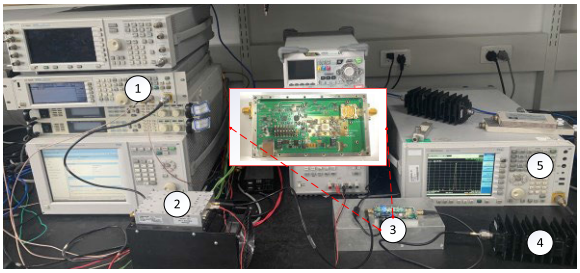

FIGURE 19. The actual test diagram.

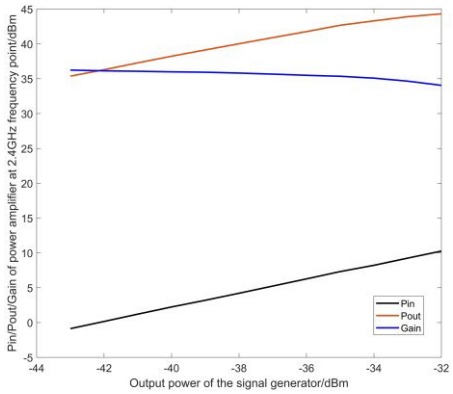

FIGURE 20. Test result 1.

As can be seen from figure 19, ① indicates the signal generator. ② shows the pre-distortion linear power amplifier. ③ indicates the bidirectional power amplifier designed in this paper. ④ indicates the attenuator. ⑤ means the spectrum meter. The relevant test data results are shown in figure 20-figure 24.

The relevant comparison results are shown in Table 1 and Table 2.

From Table 1 and Table 2, it can be intuitively seen that the 4G/5G bi-directional power amplifier designed in

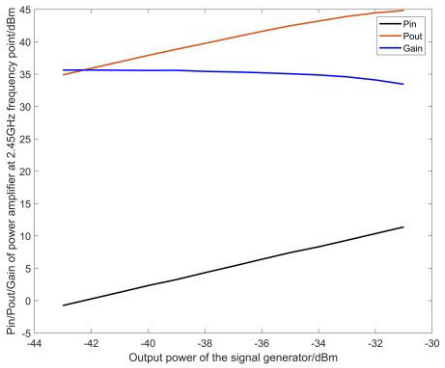

FIGURE 21. Test result 2.

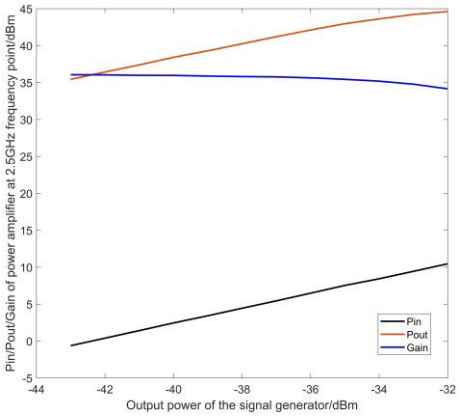

FIGURE 22. Test result 3.

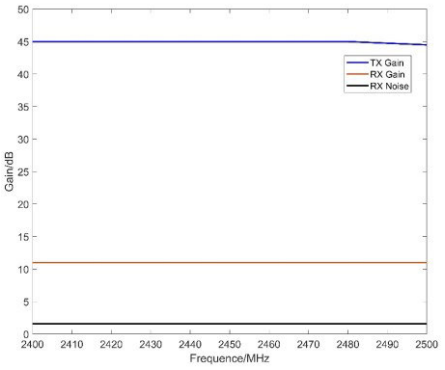

FIGURE 23. Test result 4.

this paper is far ahead of other power amplifiers in the literature regarding output power and output gain, with excellent performance. It is experimentally verified to support self-assembling wireless nodes to maintain long-spacing transmission even during high-speed movement. However, there are still some shortcomings, such as comparing with the literature [64], [65], [66], it can be found that the power amplifiers in the literature have lower operating voltages, but their output power and output gain are more objectives. Another example is comparing with the literature [62], [63], it can be found that the power amplifier in the literature can still provide efficient output power and output gain in the low

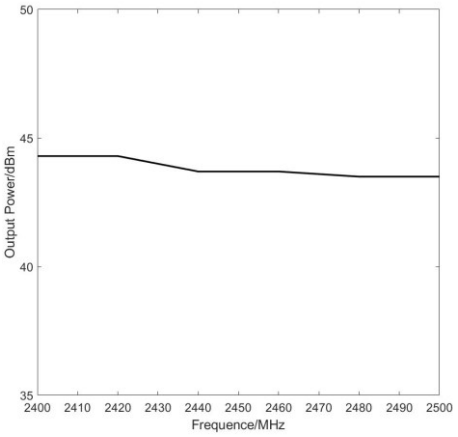

FIGURE 24. Test result 5.

TABLE 1. Comparison of performance between PA designed in this paper and PA in other literature.

	Ref[60]	Ref[61]	Ref[62]	Ref [38]	Ref [67]
Working voltage/v	3.3	3.6	3.3	3.3	3.3
Working frequency/GHz	2.4	2.4	2.4	2.4	2.4-2.5
Output power/dBm	20	18.8	29.7	23.5	30.1-30.6
Gain/dB	17.7	21.4	9.6	26.8	25.4-25.9
Whether it is applicable for the long-distance transmission and high-speed movement of amorphous flat air-to-ground Ad-Hoc network ZigBee nodes	no	no	no	Applicable, it has a specific application value but has not done relevant experiments to verify	Applicable, it has a specific application value and has done long-distance transmission experiments to verify (without high-speed movement experiments)

TABLE 2. Comparison of performance between PA designed in this paper and PA in other literature.

	Ref[63]	Ref[64]	Ref[65]	Ref[66]	**This work**
Working voltage/v	3.3	1.8	0.5	1.98	**3.6**
Working frequency/GHz	2.4	2.4	2.4	2.4	**2.4-2.5**
Output power/dBm	27.7	21.8	12.3	14.78	**41.5-43.4**
Gain/dB	28	15	none	19.75	**44**
Whether it is applicable for the long-distance transmission and high-speed movement of amorphous flat air-to-ground Ad-Hoc network ZigBee nodes	no	no	no	no	**Suitable for long-distance transmission and high-speed movement, has been verified by relevant experiments, and has particular application**

voltage state. The above two comparison results show that the 4G/5G bidirectional power amplifier designed in this paper still needs further efficiency improvement.

IV. EXPERIMENTAL TEST ANALYSIS

This test experiment includes high-speed movement and long-distance transmission of amorphous flattened air-ground wireless self-assembled network nodes. Firstly, the high-speed mobile test: includes one airborne network node and one vehicle-mounted ground network node so that the vehicle-mounted network node and the UAV airborne network node move in opposite directions to form the relative speed maximization and test the network topology. The test environment is shown in figure 25, the aerial self-grouping node is shown in figure 26, the vehicle-mounted ground self-grouping node is shown in figure 27, and the relative movement experiment test is shown in figure 28.

FIGURE 25. Experimental field.

FIGURE 26. Airborne self-organizing network nodes.

The experimental data of self-assembled network nodes moving at high speed are shown in table 3, and the relationship between the rate of self-assembled network nodes and the topology of the self-assembled network is shown in figure 29.

It can be intuitively seen in figure 29. When the relative speed is 214km/h, the network nodes can form a stable network topology, and the maximum moving speed is 123km/h due to the restricted moving speed of the vehicle ground network nodes. The UAV air network nodes are determined to move at a maximum speed of 91km/h. The limit speed value cannot be known yet, and can only be defined to support the network nodes to move at 214km/h high speed. Then the self-assembled nodes were kept moving

FIGURE 27. Terrestrial self-organizing network nodes.

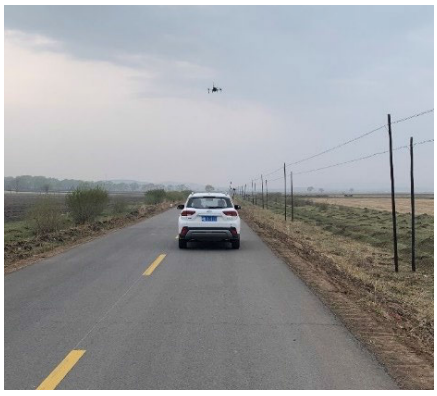

FIGURE 28. Self-assembled node high-speed mobile testing.

TABLE 3. High-speed mobile test data of self-assembled nodes.

	Ground network node speed (km/h)	Air network node speed (km/h)	Relative speed (km/h)	Network topology
1	118	91	209	Formation of stable topology
2	119	91	210	Formation of stable topology
3	120	91	211	Formation of stable topology
4	121	91	212	Formation of stable topology
5	122	91	213	Formation of stable topology
6	123	91	214	Formation of stable topology

at high speed, where the first step was not connected to the air relay node, the signal source node model was "01BA," and the signal host receiver node model was "6600". The point-to-point test was conducted. The transmission distance test data are shown in table 4, and the specific distance and the response of the self-assembled node indicator are shown in figure 30.

From figure 30, it can be seen intuitively that: when the distance is 16300 meters, the indicator light of the letter host node generally works for 5 seconds, but when the space is 16400 meters, the indicator light of the letter host node does

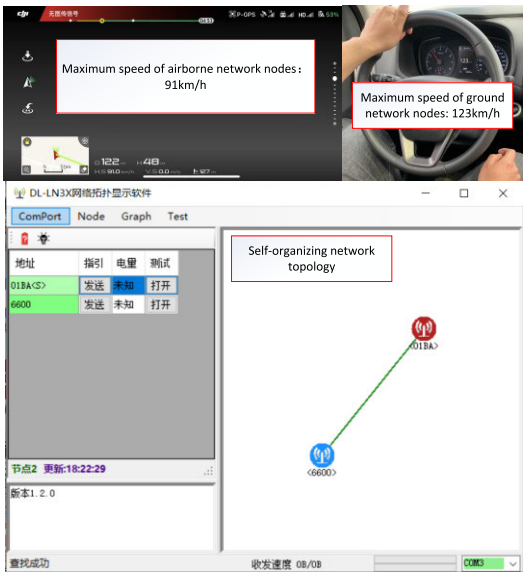

FIGURE 29. Self-assembled node high-speed mobile test topology.

TABLE 4. Experimental test results 1.

No.	Transmission distance/m	Indicator response
1	15200	The indicator light is on for 5 seconds
2	15700	The indicator light is on for 5 seconds
3	16100	The indicator light is on for 5 seconds
4	16200	The indicator light is on for 5 seconds
5	16300	The indicator light is on for 5 seconds
6	16400	The indicator light is not on and not off

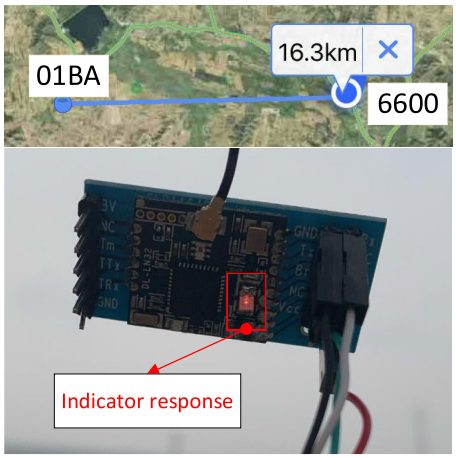

FIGURE 30. Transmission distance and indicator response of self-organizing nodes.

not light up, so the limit communication distance is between 16300-16400 meters, and here it is taken as 16300 meters. Continue to keep the self-assembling node moving at high speed, where the second step is to access the air relay node, air relay node, and ground relay node to form a common relay node. The air relay node is "65FD", the distance between the air relay node and the source node is 130 meters, and the flight height is 15 meters, and the relevant data are shown in table 5, and the experimental test results are shown in figure 31.

TABLE 5. Experimental test results 2.

No.	Transmission distance/m	Indicator response
1	18100	The indicator light is on for 5 seconds
2	19700	The indicator light is on for 5 seconds
3	22000	The indicator light is on for 5 seconds
4	24900	The indicator light is on for 5 seconds
5	25100	The indicator light is on for 5 seconds
6	25200	The indicator light is not on and not off

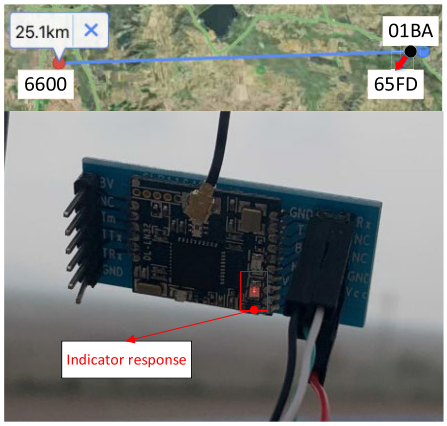

FIGURE 31. Transmission distance and indicator response of self-organizing nodes.

From figure 31, it can be seen intuitively that when the distance is 25100 meters, the indicator of the letter-host node usually works for 5 seconds. However, when the space is 25200 meters, the indicator light of the mail host node does not light up, so the limit communication distance is between 25100 and 25200 meters, which is taken as 25100 meters here. Since there are few papers and data related to the long distance between the nodes of the wireless Ad-Hoc network in 2.4GHz amorphous flat nodes, this paper only found relevant data about the test distance of the ZigBee module, and the comparative results are shown in table 6.

From table 6, it can be intuitively seen that the 4G/5G bidirectional power amplifier designed in this paper can be said to have achieved globally remarkable results in supporting long-spacing transmission of amorphous flattened air-ground wireless self-organizing network nodes for the time being, from the information collected so far. This bi-directional power amplifier can realize the long-range wireless transmission of 16,300 meters for the ground point-to-point of wireless self-organizing network nodes and the long-range wireless communication of 25,100 meters for the air-ground integration of wireless self-organizing network nodes after the introduction of UAVs. This paper provides a specific research basis for the subsequent terahertz long-range transmission and wireless charging.

V. DISCUSSION AND SPECIAL NOTES

This paper designs a bi-directional power amplifier for long-spacing transmission of air-ground wireless networking nodes under high-speed movement. However, it does not

TABLE 6. Comparing the results.

Reference	Working frequency/GHz	Whether to support high-speed mobile	The max transmission distance /m
Ref[68]	2.4GHz	Uncertain	100
Ref[69]	2.4GHz	Uncertain	140
Ref[70]	2.4GHz	Uncertain	350
Ref[71]	2.4GHz	Uncertain	500
Ref[72]	2.4GHz	Uncertain	600
Ref[73]	2.4GHz	Uncertain	800
Ref[74]	433MHz	Uncertain	1000
Ref[49]	2.4GHz	Uncertain	1142.1
Ref[75]	2.4GHz	Uncertain	1200
Ref[76]	868MHz	Uncertain	2200
Ref[77]	2.4GHz	Uncertain	2200
Ref[78]	2.4GHz	Uncertain	4200
Ref[79]	2.4GHz	Uncertain	6020
Ref[80]	2.4GHz	Uncertain	6500
Ref[81]	2.4GHz	Support	7665
Ref[67]	2.4GHz	Uncertain	9600-14800
This work is about ground Ad-Hoc network nodes	**2.4GHz**	**Support**	**16300**
This work about air-to-ground Ad-Hoc network nodes	**2.4GHz**	**Support**	**25100**

mention air-ground networking communication, air-ground bi-directional relay beamforming noise interference, and air-ground networking information collision in the paper, so we make the following relevant special notes here.

The authors of this paper have been devoted to the research of long-spacing transmission under the high-speed movement of amorphous flattened air-ground wireless self-assembled network nodes and have achieved specific research results in collaborative beamforming of air-ground relays, optimization of air-ground bidirectional noise balance, and virtual MIMO non-sensitive filtering, among which the main contributions are as follows.

(1) Z. Wang, J. Dong, J. Yu, Z. Yu, S. Lin, and K. Li, "The Air-Ground Integrated MIMO Cooperative Relay Beamforming Wireless Ad-Hoc Network Technology Research That Based on Maximum Ratio Combining," 2020 International Workshop on Electronic Communication and Artificial Intelligence (IWECAI), 2020, pp. 11-19, DOI: 10.1109/IWECAI50956.2020.00010.

Paper (1) proposes an air-ground relay collaborative forwarding amplified beamforming model with an MRC diversity acceptance technique at the host node and optimally solves the problem of reducing the false bit rate as the SNR increases by using convex optimization. Based on the collaborative communication and MIMO system with multiple antenna system gain in modern wireless communication networks, we propose an integrated air-ground relaying and amplifying base station platform and a more realistic solution to the problem of correlated noise introduced by multiple wireless self-assembling network relay nodes and signals from interference sources received by the relay nodes and the host nodes, which affect the SNR of the system. The proposed method is based on the convex optimization method to solve the air-ground relay beamforming vector, and the signal received at the host node is performed by MRC diversity.

(2) Wang, ZF; Yu, JG; Bi, K; Lin, SJ; Yu, Z. Research on Long-distance Transmission of Nodes in Amorphous Flat Air-to-ground Wireless Ad-Hoc Network Based on Bidirectional Relay Beamforming[J] Ad Hoc & Sensor Wireless Networks. 2022,51:41-59.

Paper (2) proposes the optimal solution strategy of signal-to-noise ratio balance for two-way relay beamforming based on one-way relay beamforming so that when the system faces external noise interference, its SNR can still be in a good state and has good balance and controllability.

(3) Zhifang Wang, Jianguo Yu, Zhiyao Wang, Shangjing Lin. Bidirectional Robust and Fault-tolerant H_∞ Non-sensitive Compensation Filter Controller based on Amorphous Flattened Air-to-ground Wireless Self-assembly System[J]. ISA Transactions. 2023, 132: 508-523. DOI: 10.1016/j.isatra.2022.05.043.

Paper (3) designs a bi-directional robust fault-tolerant non-sensitive compensated filter controller based on the powerful adaptive fault-tolerant control algorithm. The LMI method enables the designed filter controller to further optimize the fault-tolerance correction factor and the robust adaptive factor under the regulation of the feedback matrix K so that the system estimation error asymptotically converges to zero and then can simultaneously solve the optimization problems of unknown faults (including external disturbances, partial failures of internal actuators and random interruptions) of the self-assembled nodes and the acquisition of SNR by the self-assembled wireless nodes.

The paper (1-3) makes more detailed explanations in the field of relay selection analysis for an opportunistic two-hop multi-user system in a Poisson field of nodes or multi-user beamforming and ground station deployment for 5G direct air-to-ground communication. This paper is a further study based on the authors' previous research, focusing mainly on the study of RF power amplifiers for amorphous flattened air-ground wireless self-assembling network systems, so not much elaboration is made in the aspects of air-ground self-assembling wireless network communication, etc., and particular explanations are made here.

VI. CONCLUSION

In this paper, we designed a power amplifier to support the long-range transmission of amorphous flat air-to-ground wireless self-organizing network nodes during high-speed movement. Comprehensive simulation and experimental test verification analysis show that the wireless self-organizing network nodes can support 25.1km point-to-point long-range transmission at a relative speed of 214km/h when the designed power amplifier is added to the amorphous flat air-to-ground wireless self-organizing network system. The research work in this paper is of great significance in that it

can significantly reduce the cost of wireless self-organizing network coverage while improving the node's performance in all aspects, but how to reduce the size and weight of the device is still a problem that needs to be optimized. This paper provides a specific research basis for realizing a framework system for low-altitude economic fly-by-wire networking in the future.

CONFLICT OF INTERSET

The authors declare no conflict of interest.

REFERENCES

[1] R. Wu and Q.-X. Chu, "A compact, dual-polarized multiband array for 2G/3G/4G base stations," *IEEE Trans. Antennas Propag.*, vol. 67, no. 4, pp. 2298–2304, Apr. 2019, doi: 10.1109/TAP.2019.2902652.

[2] B. A. Elono Ongbwa, A. D. Kora, and T. J. Fotso Wabo, "Improvement of special drive test route (SDTR) reliability for indoor radio frequency coverage assessment in 3G/4G mobile networks," in *Proc. 22nd Int. Conf. Adv. Commun. Technol. (ICACT)*, Feb. 2020, pp. 222–227, doi: 10.23919/ICACT48636.2020.9061361.

[3] C. Ge, N. Wang, I. Selinis, J. Cahill, M. Kavanagh, K. Liolis, C. Politis, J. Nunes, B. Evans, Y. Rahulan, and N. Nouvel, "QoE-assured live streaming via satellite backhaul in 5G networks," *IEEE Trans. Broadcast.*, vol. 65, no. 2, pp. 381–391, Jun. 2019, doi: 10.1109/TBC.2019.2901397.

[4] A. Ghosh, A. Maeder, M. Baker, and D. Chandramouli, "5G evolution: A view on 5G cellular technology beyond 3GPP release 15," *IEEE Access*, vol. 7, pp. 127639–127651, 2019, doi: 10.1109/ACCESS.2019.2939938.

[5] W. Hong, Z. H. Jiang, C. Yu, D. Hou, H. Wang, C. Guo, Y. L. Hu Kuai, Y. Yu, Z. Jiang, Z. Chen, J. Chen, Z. Yu, J. Zhai, N. Zhang, L. Tian, F. Wu, G. Yang, Z.-C. Hao, and J. Y. Zhou, "The role of millimeter-wave technologies in 5G/6G wireless communications," *IEEE J. Microw.*, vol. 1, no. 1, pp. 101–122, Jan. 2021, doi: 10.1109/JMW.2020.3035541.

[6] H. Viswanathan and P. E. Mogensen, "Communications in the 6G era," *IEEE Access*, vol. 8, pp. 57063–57074, 2020, doi: 10.1109/ACCESS.2020.2981745.

[7] I. F. Akyildiz, A. Kak, and S. Nie, "6G and beyond: The future of wireless communications systems," *IEEE Access*, vol. 8, pp. 133995–134030, 2020, doi: 10.1109/ACCESS.2020.3010896.

[8] J.-L. Yao, Y.-Z. Sun, H.-P. Ren, and C. Grebogi, "Experimental wireless communication using chaotic baseband waveform," *IEEE Trans. Veh. Techn.*, vol. 68, no. 1, pp. 578–591, Jan. 2019, doi: 10.1109/TVT.2018.2882422.

[9] J. Huang, C.-X. Wang, H. Chang, J. Sun, and X. Q. Gao, "Multi-frequency multi-scenario millimeter wave MIMO channel measurements and modeling for B5G wireless communication systems," *IEEE J. Sel. Areas Commun.*, vol. 38, no. 9, pp. 2010–2025, Sep. 2020, doi: 10.1109/JSAC.2020.3000839.

[10] F. Wu, W. Yang, R. Chen, and X. Xie, "Broadband communications for high-speed trains via NDN wireless mesh network," *Tsinghua Sci. Technol.*, vol. 23, no. 4, pp. 419–430, Aug. 2018, doi: 10.26599/TST.2018.9010046.

[11] Sharavanan and R. M. Balajee, "Junction based urban scenario high speed node detection (JBUS-HSND) and alerting system on VANET," in *Proc. Int. Conf. Recent Trends Inf. Technol. (ICRTIT)*, Apr. 2016, pp. 1–6, doi: 10.1109/ICRTIT.2016.7569512.

[12] D. Zhou, T. Shi, X. Lv, and W. Bai, "A research on banded topology control of wireless sensor networks along high-speed railways," in *Proc. 34th Chin. Control Conf. (CCC)*, Jul. 2015, pp. 7736–7740, doi: 10.1109/ChiCC.2015.7260868.

[13] D. Kang, W. Wang, B. Eon Park, L. Xing, and S. Shin, "NS-2 based wireless vehicular network performance study with high speed urban mobile relays," in *Proc. 7th Int. Conf. Commun. Netw. China*, Aug. 2012, pp. 591–595, doi: 10.1109/ChinaCom.2012.6417552.

[14] V. Barinov, A. Smirnov, and D. Migalin, "Modified protocol for data transmission in ad-hoc networks with high speed objects using directional antennas," in *Proc. 9th East-West Design Test Symp. (EWDTS)*, Sep. 2011, pp. 150–153, doi: 10.1109/EWDTS.2011.6116586.

[15] A. Gaynulin and V. Krylov, "Dynamic resource allocation in ad-hoc hybrid high-speed wireless networks," in *Proc. 2nd Int. Conf. Inf. Commun. Technol.*, 2006, pp. 2461–2466, doi: 10.1109/ICTTA.2006.1684793.

[16] Y. Luo, X. Su, Y. Yu, Q. Cao, and Z. Ni, "Real-time successful broadcasting ratio and distance based broadcast for vehicular ad hoc networks," in *Proc. Int. Conf. Wireless Commun. Signal Process. (WCSP)*, Oct. 2020, pp. 1046–1051, doi: 10.1109/WCSP49889.2020.9299727.

[17] M. M. Shawara, A. M. Sarhan, and N. A. Elfishawy, "Energy aware ad-hoc on demand multipath distance vector (EA-AOMDV)," in *Proc. 13th Int. Comput. Eng. Conf. (ICENCO)*, Dec. 2017, pp. 317–322, doi: 10.1109/ICENCO.2017.8289807.

[18] C. Pu, "Jamming-resilient multipath routing protocol for flying ad hoc networks," *IEEE Access*, vol. 6, pp. 68472–68486, 2018, doi: 10.1109/ACCESS.2018.2879758.

[19] B. H. Khudayer, M. Anbar, S. M. Hanshi, and T.-C. Wan, "Efficient route discovery and link failure detection mechanisms for source routing protocol in mobile ad-hoc networks," *IEEE Access*, vol. 8, pp. 24019–24032, 2020, doi: 10.1109/ACCESS.2020.2970279.

[20] O. N. Samijayani, R. Darwis, S. Rahmatia, A. Mujadin, and D. Astharini, "Hybrid ZigBee and WiFi wireless sensor networks for hydroponic monitoring," in *Proc. Int. Conf. Electr., Commun., Comput. Eng. (ICECCE)*, Jun. 2020, pp. 1–4, doi: 10.1109/ICECCE49384.2020.9179342.

[21] H. Pirayesh, P. K. Sangdeh, and H. Zeng, "Securing ZigBee communications against constant jamming attack using neural network," *IEEE Internet Things J.*, vol. 8, no. 6, pp. 4957–4968, Mar. 2021, doi: 10.1109/JIOT.2020.3034128.

[22] Z. Chi, Y. Li, H. Sun, Z. Huang, and T. Zhu, "Simultaneous bi-directional communications and data forwarding using a single ZigBee data stream," *IEEE/ACM Trans. Netw.*, vol. 29, no. 2, pp. 821–833, Apr. 2021, doi: 10.1109/TNET.2021.3054339.

[23] Z. Wang, Y. Cao, L. Kong, G. Chen, J. Yu, S. Tang, and Y. Chen, "Reference waveforms forward concurrent transmissions in ZigBee communications," *IEEE/ACM Trans. Netw.*, vol. 28, no. 4, pp. 1629–1642, Aug. 2020, doi: 10.1109/TNET.2020.2992271.

[24] X. Zhang, K.-D. Hong, L. Zhu, X.-K. Bi, and T. Yuan, "Wideband differentially fed patch antennas under dual high-order modes for stable high gain," *IEEE Trans. Antennas Propag.*, vol. 69, no. 1, pp. 508–513, Jan. 2021, doi: 10.1109/TAP.2020.3006394.

[25] P. Mei, S. Zhang, and G. F. Pedersen, "A dual-polarized and high-gain X-/Ka-band shared-aperture antenna with high aperture reuse efficiency," *IEEE Trans. Antennas Propag.*, vol. 69, no. 3, pp. 1334–1344, Mar. 2021, doi: 10.1109/TAP.2020.3026429.

[26] E. Baldazzi, A. Al-Rawi, R. Cicchetti, A. B. Smolders, O. Testa, C. D. J. V. C. Moreno, and D. Caratelli, "A high-gain dielectric resonator antenna with plastic-based conical horn for millimeter-wave applications," *IEEE Antennas Wireless Propag. Lett.*, vol. 19, no. 6, pp. 949–953, Jun. 2020, doi: 10.1109/LAWP.2020.2984565.

[27] K. Gumber and M. Rawat, "Low-cost RF_{in}–RF_{out} predistorter linearizer for high-power amplifiers and ultra-wideband signals," *IEEE Trans. Instrum. Meas.*, vol. 67, no. 9, pp. 2069–2081, Sep. 2018, doi: 10.1109/TIM.2018.2811420.

[28] P. Jia, F. You, and S. He, "A 1.8–3.4-GHz bandwidth-improved reconfigurable mode Doherty power amplifier utilizing switches," *IEEE Microw. Wireless Compon. Lett.*, vol. 30, no. 1, pp. 102–105, Jan. 2020, doi: 10.1109/LMWC.2019.2951215.

[29] C. Liang, J. I. Martinez-Lopez, P. Roblin, Y. Hahn, D. Mikrut, and V. Chen, "Wideband two-way hybrid Doherty outphasing power amplifier," *IEEE Trans. Microw. Theory Techn.*, vol. 69, no. 2, pp. 1415–1428, Feb. 2021, doi: 10.1109/TMTT.2020.3019430.

[30] D. Jiang, L. Huo, and H. Song, "Rethinking behaviors and activities of base stations in mobile cellular networks based on big data analysis," *IEEE Trans. Netw. Sci. Eng.*, vol. 7, no. 1, pp. 80–90, Jan. 2020, doi: 10.1109/TNSE.2018.2861388.

[31] K. Feng and M. Haenggi, "On the location-dependent SIR gain in cellular networks," *IEEE Wireless Commun. Lett.*, vol. 8, no. 3, pp. 777–780, Jun. 2019, doi: 10.1109/LWC.2019.2892422.

[32] O. Sadio, I. Ngom, and C. Lishou, "Controlling WiFi direct group formation for non-critical applications in C-V2X network," *IEEE Access*, vol. 8, pp. 79947–79957, 2020, doi: 10.1109/ACCESS.2020.2990671.

[33] N. Adam, C. Tapparello, and W. Heinzelman, "Performance evaluation of WiFi direct multi hop ad-hoc networks," in *Proc. Int. Conf. Comput., Netw. Commun. (ICNC)*, Feb. 2020, pp. 661–666, doi: 10.1109/ICNC47757.2020.9049743.

[34] G. Klimiashvili, C. Tapparello, and W. Heinzelman, "LoRa vs. WiFi ad hoc: A performance analysis and comparison," in *Proc. Int. Conf. Comput., Netw. Commun. (ICNC)*, Feb. 2020, pp. 654–660, doi: 10.1109/ICNC47757.2020.9049724.

[35] L. You, J. Xiong, D. W. K. Ng, C. Yuen, W. Wang, and X. Gao, "Energy efficiency and spectral efficiency tradeoff in RIS-aided multiuser MIMO uplink transmission," *IEEE Trans. Signal Process.*, vol. 69, pp. 1407–1421, 2020, doi: 10.1109/TSP.2020.3047474.

[36] L. You, J. Xiong, A. Zappone, W. Wang, and X. Gao, "Spectral efficiency and energy efficiency tradeoff in massive MIMO downlink transmission with statistical CSIT," *IEEE Trans. Signal Process.*, vol. 68, pp. 2645–2659, 2020, doi: 10.1109/TSP.2020.2986391.

[37] J. Ghosh, "A trade-off between energy efficiency and spectral efficiency in macro-femtocell networks," *IEEE Trans. Veh. Technol.*, vol. 69, no. 10, pp. 10914–10924, Oct. 2020, doi: 10.1109/TVT.2019.2937920.

[38] D. Manente, F. Padovan, D. Seebacher, M. Bassi, and A. Bevilacqua, "A 28-GHz stacked power amplifier with 20.7-dBm output P1dB in 28-nm bulk CMOS," *IEEE Solid-State Circuits Lett.*, vol. 3, pp. 170–173, 2020, doi: 10.1109/LSSC.2020.3009973.

[39] C. Wan, H. Zhang, L. Li, and K. Wang, "A 30-to-41 GHz SiGe power amplifier with optimized cascode transistors achieving 22.8 dBm output power and 27% PAE," *IEEE Trans. Circuits Syst. II, Exp. Briefs*, vol. 68, no. 4, pp. 1158–1162, Apr. 2021, doi: 10.1109/TCSII.2020.3035936.

[40] P. Starke, C. Carta, and F. Ellinger, "High-linearity 19-dB power amplifier for 140–220 GHz, saturated at 15 dBm, in 130-nm SiGe," *IEEE Microw. Wireless Compon. Lett.*, vol. 30, no. 4, pp. 403–406, Apr. 2020, doi: 10.1109/LMWC.2020.2978397.

[41] H. Lyu and K. Chen, "Balanced-to-Doherty mode-reconfigurable power amplifier with high efficiency and linearity against load mismatch," *IEEE Trans. Microw. Theory Techn.*, vol. 68, no. 5, pp. 1717–1728, May 2020, doi: 10.1109/TMTT.2020.2979844.

[42] W.-R. Fang, W.-H. Huang, W.-H. Huang, J.-W. Li, C. Fu, L.-L. Wang, T.-W. He, and Y. Cao, "X-band high-efficiency high-power GaN power amplifier based on edge-triggered gate modulation," *IEEE Microw. Wireless Compon. Lett.*, vol. 30, no. 9, pp. 884–887, Sep. 2020, doi: 10.1109/LMWC.2020.3013146.

[43] M. Gilasgar, A. Barlabe, and L. Pradell, "High-efficiency reconfigurable dual-band class-F power amplifier with harmonic control network using MEMS," *IEEE Microw. Wireless Compon. Lett.*, vol. 30, no. 7, pp. 677–680, Jul. 2020, doi: 10.1109/LMWC.2020.2994373.

[44] T.-H. Fan, Y. Wang, and H. Wang, "A broadband transformer-based power amplifier achieving 24.5-dBm output power over 24–41 GHz in 65-nm CMOS process," *IEEE Microw. Wireless Compon. Lett.*, vol. 31, no. 3, pp. 308–311, Mar. 2021, doi: 10.1109/LMWC.2020.3040786.

[45] P. Zurek, T. Cappello, and Z. Popovic, "Broadband diplexed power amplifier," *IEEE Microw. Wireless Compon. Lett.*, vol. 30, no. 11, pp. 1073–1076, Nov. 2020, doi: 10.1109/LMWC.2020.3026050.

[46] M. Kalcher, D. Gruber, and D. Ponton, "1–3-GHz self-aligned open-loop local quadrature phase generator with phase error below 0.4°," *IEEE Trans. Microw. Theory Techn.*, vol. 68, no. 8, pp. 3510–3518, Aug. 2020, doi: 10.1109/TMTT.2020.3001651.

[47] P. Frigerio, M. Gianollo, G. Pezzi, L. Molinari, A. Barbieri, M. Zamprogno, R. Carminati, N. Boni, and G. Langfelder, "Mitigating hysteresis effects in open-loop-driven PZT MEMS micromirrors with piezoresistive sensing," in *Proc. 21st Int. Conf. Solid-State Sensors, Actuat. Microsystems (Transducers)*, Jun. 2021, pp. 1100–1103, doi: 10.1109/Transducers50396.2021.9495403.

[48] S. H. M. Torres, P. G. E. Meneses, and A. C. J. Pesántez, "Implementation of a low cost smart home based on standard 802.11 b/g/n WiFi," in *Proc. 7th Int. Eng., Sci. Technol. Conf. (IESTEC)*, Oct. 2019, pp. 520–525, doi: 10.1109/IESTEC46403.2019.00099.

[49] Z. Wang, J. Dong, J. Yu, Z. Yu, S. Lin, and K. Li, "The air-ground integrated MIMO cooperative relay beamforming wireless ad-hoc network technology research that based on maximum ratio combining," in *Proc. Int. Workshop Electron. Commun. Artif. Intell. (IWECAI)*, Jun. 2020, pp. 11–19, doi: 10.1109/IWECAI50956.2020.00010.

[50] K. Sohraby, D. Minoli, and T. Znati, "Wireless transmission technology and systems," in *Wireless Sensor Networks: Technology, Protocols, and Applications*. Hoboken, NJ, USA: Wiley, 2007, pp. 93–141, doi: 10.1002/9780470112762.ch4.

[51] A. Sendin, J. Matanza, and R. Ferrus, "Wireless IoT technologies," in *Smart Grid Telecommunications: Fundamentals and Technologies in the 5G Era*. 2021, pp. 293–337, doi: 10.1002/9781119755401.ch8.

[52] J. Liu, Z. Wang, and L. Zhang, "Integrated vehicle-following control for four-wheel-independent-drive electric vehicles against non-ideal V2X communication," *IEEE Trans. Veh. Technol.*, vol. 71, no. 4, pp. 3648–3659, Apr. 2022, doi: 10.1109/TVT.2022.3141732.

[53] J. Zhou, D. Tian, Y. Wang, Z. Sheng, X. Duan, and V. C. M. Leung, "Reliability-optimal cooperative communication and computing in connected vehicle systems," *IEEE Trans. Mobile Comput.*, vol. 19, no. 5, pp. 1216–1232, May 2020, doi: 10.1109/TMC.2019.2907491.

[54] Y. Fang, H. Min, X. Wu, W. Wang, X. Zhao, and G. Mao, "On-ramp merging strategies of connected and automated vehicles considering communication delay," *IEEE Trans. Intell. Transp. Syst.*, vol. 23, no. 9, pp. 15298–15312, Sep. 2022, doi: 10.1109/TITS.2022.3140219.

[55] W. Jia, Y. Cao, S. Zhang, and W.-Q. Wang, "Detecting high-speed maneuvering targets by exploiting range-Doppler relationship for LFM radar," *IEEE Trans. Veh. Technol.*, vol. 70, no. 3, pp. 2209–2218, Mar. 2021, doi: 10.1109/TVT.2021.3057364.

[56] Z. Gong, C. Li, F. Jiang, and M. Z. Win, "Data-aided Doppler compensation for high-speed railway communications over mmWave bands," *IEEE Trans. Wireless Commun.*, vol. 20, no. 1, pp. 520–534, Jan. 2021, doi: 10.1109/TWC.2020.3026158.

[57] R. Wei, X. Ma, S. Zhao, and S. Yan, "Doppler estimation based on dual-HFM signal and speed spectrum scanning," *IEEE Signal Process. Lett.*, vol. 27, pp. 1740–1744, 2020, doi: 10.1109/LSP.2020.3020222.

[58] A. A. Doroshkin, A. M. Zadorozhny, O. N. Kus, V. Y. Prokopyev, and Y. M. Prokopyev, "Experimental study of LoRa modulation immunity to Doppler effect in CubeSat radio communications," *IEEE Access*, vol. 7, pp. 75721–75731, 2019, doi: 10.1109/ACCESS.2019.2919274.

[59] J. Millman and A. Grabel, *Microelectronics*, 2nd ed. New York, NY, USA: McGraw-Hill, 1987.

[60] F. Forni, Y. Shi, H. P. A. van den Boom, E. Tangdiongga, and A. M. J. Koonen, "Multiband LTE—A, WiFi AC, and 4-PAM baseband simultaneous transmission over 50 M thick-core POF for in-home network," in *Proc. 19th Int. Conf. Transparent Opt. Netw. (ICTON)*, Jul. 2017, pp. 1–4, doi: 10.1109/ICTON.2017.8025158.

[61] A. D. Kora and V. N. Tezo, "Design and implementation of low-cost microwave full-duplex system based on WiFi cards for transmission over a long distance," in *Proc. 13th Int. Conf. Adv. Commun. Technol. (ICACT2011)*, Gangwon, South Korea, 2011, pp. 1331–1334.

[62] P. Jia, F. You, and S. He, "A 1.8–3.4-GHz bandwidth-improved reconfigurable mode Doherty power amplifier utilizing switches," *IEEE Microw. Wireless Compon. Lett.*, vol. 30, no. 1, pp. 102–105, Jan. 2020, doi: 10.1109/LMWC.2019.2951215.

[63] C. Lang, Y. Jianlian, and G. Yebing, "The utility model relates to a 2.4 GHz CMOS RF front-end circuit," *Microelectronics*, vol. 47, no. 5, pp. 20–24, 2017.

[64] C.-Y. Lin and G.-Y. Li, "ESD protection design for open-drain power amplifier in CMOS technology," *IEEE Trans. Device Mater. Rel.*, vol. 19, no. 4, pp. 782–790, Dec. 2019, doi: 10.1109/TDMR.2019.2951939.

[65] A. F. Aref, R. Negra, and M. A. Khan, "Class-0: A highly linear class of power amplifier in 0.13μm CMOS for WCDMA/LTE applications," in *IEEE Int. Solid-State Circuits Conf. (ISSCC) Dig. Tech. Papers*, San Francisco, CA, USA, Feb. 2015, pp. 1–3.

[66] C. Fuzhan, L. Yanbin, G. Yebing, and Y. Jianlian, "A 2.4 GHz CMOS power amplifier with adaptive bias circuit," *Microelectronics*, vol. 50, no. 6, pp. 817–822, 2020.

[67] Z. Wang, J. Yu, K. Bi, W. Zhu, and S. Lin, "A 2.4 GHz bidirectional power amplifier extending nodes distance of transmission to 14.8 km for amorphous flat air-to-ground wireless ad hoc network," *Arabian J. Sci. Eng.*, vol. 47, no. 3, pp. 3239–3254, Mar. 2022, doi: 10.1007/s13369-021-06089-2.

[68] P. D. P. Adi, V. Sihombing, V. M. M. Siregar, G. J. Yanris, F. A. Sianturi, W. Purba, S. P. Tamba, J. Simatupang, R. Arifuddin, Subairi, and D. A. Prasetya, "A performance evaluation of ZigBee mesh communication on the Internet of Things (IoT)," in *Proc. 3rd East Indonesia Conf. Comput. Inf. Technol. (EIConCIT)*, Apr. 2021, pp. 7–13, doi: 10.1109/EIConCIT50028.2021.9431875.

[69] T. Li, H. Abe, S. Tateno, and Y. Hachiya, "Comparison of wireless communication technologies in remote monitoring systems," in *Proc. 18th Int. Conf. Control, Autom. Syst. (ICCAS)*, PyeongChang, South Korea, 2018, pp. 591–595.

[70] Z. Li and T. He, "LongBee: Enabling long-range cross-technology communication," in *Proc. IEEE Conf. Comput. Commun.*, Apr. 2018, pp. 162–170, doi: 10.1109/INFOCOM.2018.8485938.
[71] W. Yuan, C. Keshan, X. Chao, and L. Hongjian, "Design and implementation for ZigBee long-distance wireless data transmission system," in *Proc. IEEE 10th Int. Conf. Electron. Meas. Instrum.*, Chengdu, China, Aug. 2011, pp. 61–64, doi: 10.1109/ICEMI.2011.6037679.
[72] Z. Li and Y. Chen, "BLE2LoRa: Cross-technology communication from Bluetooth to LoRa via chirp emulation," in *Proc. 17th Annu. IEEE Int. Conf. Sens., Commun., Netw. (SECON)*, Jun. 2020, pp. 1–9, doi: 10.1109/SECON48991.2020.9158446.
[73] F. Righetti, C. Vallati, D. Comola, and G. Anastasi, "Performance measurements of IEEE 802.15.4g wireless networks," in *Proc. IEEE 20th Int. Symp. World Wireless, Mobile Multimedia Networks (WoWMoM)*, Jun. 2019, pp. 1–6, doi: 10.1109/WoWMoM.2019.8793051.
[74] S. Dasiga, A. A. R. Bhatia, A. Bhirangi, and A. Siddiqua, "LoRa for the last mile connectivity in IoT," in *Proc. 9th Int. Conf. Syst. Model. Advancement Res. Trends (SMART)*, Dec. 2020, pp. 195–200, doi: 10.1109/SMART50582.2020.9337114.
[75] J. Niu, R. Zhang, G. Wang, S. Li, and S. Wan, "Design and experimental evaluation of long-distance and high-mobility ZigBee transceivers for WSNs," in *Proc. IEEE/CIC Int. Conf. Commun. China Workshops (CIC/ICCC)*, Aug. 2013, pp. 142–147, doi: 10.1109/ICCChinaW.2013.6670583.
[76] S. Biswas, K. P. Y. Marzuk, E. Bhardwaj, and S. Santhosh, "The firefly unit: A MANET based communication system using ZigBee and LoRaWAN protocols for IoT applications in remote locations," in *Proc. Int. Conf. Advance Comput. Innov. Technol. Eng. (ICACITE)*, Mar. 2021, pp. 642–646, doi: 10.1109/ICACITE51222.2021.9404591.
[77] Z. F. Wang, J. G. Yu, K. Bi, S. J. Lin, and Z. Yu, "Research on long-distance transmission of nodes in amorphous flat air-to-ground wireless ad-hoc network based on bidirectional relay beamforming," *Ad Hoc Sensor Wireless Netw.*, vol. 51, nos. 1–3, pp. 41–59, 2022.
[78] Z. Wang, J. Yu, and S. Lin, "Bidirectional robust and fault-tolerant H∞ non-sensitive compensation filter controller based on amorphous flattened air-to-ground wireless self-assembly system," *ISA Trans.*, vol. 132, pp. 508–523, Jan. 2023, doi: 10.1016/j.isatra.2022.05.043.
[79] G. Hongfu, B. Lina, and G. Zhihua, "Estimation method for the transmission distance for the 2.4 GHz ZigBee application," *J. Xidian Univ.*, vol. 36, no. 4, pp. 691–696, 2009.
[80] V. Sittakul, S. Pasakawee, and P. Kovintavewat, "Data transmission of ZigBee over fiber," in *Proc. 34th Int. Tech. Conf. Circuits/Systems, Comput. Commun. (ITC-CSCC)*, Jeju, South Korea, Jun. 2019, pp. 1–4, doi: 10.1109/ITC-CSCC.2019.8793406.
[81] Z. Wang, J. Yu, and S. Lin, "High-speed mobile real-time topology optimization of amorphous flattened air-to-ground wireless self-organizing network nodes based on dynamic planning," in *Proc. 3rd Int. Conf. Electron. Commun., Netw. Comput. Technol. (ECNCT)*, Xiamen, China, Mar. 2022.

ZHIFANG WANG received the Ph.D. degree in electronics and communication engineering from the Beijing University of Posts and Telecommunications (BUPT), Beijing, in 2022. He is currently a Lecturer with the Henan University of Engineering. His research interests include networked robust fault tolerant control for wireless communication systems and amorphous *ad-hoc* network design.

QUANZHEN HUANG received the M.S. degree in control science from Henan Polytechnic University, China, in 2009, and the Ph.D. degree in control science from Shanghai University, China, in 2012. He is currently a Professor with the School of Electrical Information Engineering, Henan Institute of Engineering, China. His research interests include control science and mobile edge computing.

JIANGUO YU received the Ph.D. degree in electromagnetic field and microwave technology from the Beijing University of Posts and Telecommunications (BUPT), Beijing, in 1997. After graduation, he worked for 15 years with the Fiberhome Technology Group. He was an engineer, a senior engineer, and a professor-level senior engineer. He has long-term research on microwave, millimeter wave, terahertz wave, and light wave. He is responsible for completing the 3G/4G base station, fiber remote base station, digital fiber optic repeater, 3G/4G signal source, development, and conversion of the frequency sweeper and winning the bid for China Telecom, China Mobile, and China Unicom. He was elected to the National 863 Expert Group, in April 1999. He was the Deputy Head of the overall group of major cross-themes of the optoelectronics, communication, and computer networks and a full-time overall group member. He designed and established the world's first multi-vendor equipment interconnection and mutual interoperability. Operation, unified high-speed information optical network for network management. He is currently a Professor with the Beijing University of Posts and Telecommunications and a Ph.D. Tutor.